Signatures of phase coherence in the low-temperature transport properties of multiwall carbon nanotubes

Zhengfan Zhang and Venkat Chandrasekhar*
Department of Physics and Astronomy, Northwestern University, Evanston, Illinois 60208, USA
(Received 23 August 2005; published 14 February 2006)

Four-terminal low-temperature measurements of the electrical transport of multiwall carbon nanotube devices with low-resistance contacts reveal features that signify the presence of phase coherent transport. Sharp resonances in the differential resistance as a function of dc bias are observed that are due to the interference of electron paths that are directly transmitted through the nanotube and paths that are transmitted via resonant states, the so-called Fano resonance. The metastability of these resonances indicates that the resonant states most likely arise from potentials created by metastable defects in the device. Correlations between the nanotube conductance and the simultaneously measured conductance of the contacts hint that the defects may be located at the contacts, although the nonlocality introduced by the long-range phase coherence makes an absolute determination of the location of the impurities by this technique impossible.

DOI: 10.1103/PhysRevB.73.075421 PACS number(s): 73.63.Fg, 85.35.Kt, 73.20.Hb

Quantum transport in carbon nanotubes has attracted tremendous attention due to the unique one-dimensional nature of these materials. While there have been some indications of ballistic transport in multiwalled carbon nanotubes (MWNTs),[1,2] most experiments have shown typical manifestations of phase coherent quantum transport in the diffusive regime such as weak localization, conductance fluctuations and $h/2e$-periodic Aharonov-Bohm oscillations.[3–12] The phase-coherence lengths inferred from these measurements are short in comparison to those found in metals at low temperature, ranging from a few tens of nanometers to a few hundred nanometers. However, other experiments have found magnetotransport behavior in MWNT devices that is inconsistent with diffusive quantum transport.[13] These results have been interpreted as arising from the effect of the magnetic field on the band structure in the ballistic regime, although this interpretation is not without controversy.[14]

In this paper, we give details of our experiments on quantum interference effects in MWNT devices with low-resistance contacts.[15] The devices show classic signatures of phase-coherent transport at low temperatures, including large variations in the conductance with magnetic field and a magnetoconductance that is asymmetric in the magnetic field, consistent with the Landauer-Büttiker theory of four-terminal phase-coherent transport.[16,17] However, the most striking aspect of the low-temperature transport properties of these devices is the presence of peaks and valleys in the differential conductance as a function of dc bias across the device. These peaks and valleys grow in amplitude with decreasing temperature and can change as a function of thermal cycling and even as a function of time, suggesting that they are due to metastable impurities or defects. A model based on Fano resonances arising from the interference of electrons directly transmitted through the nanotube and those transmitted via resonant states arising from the defect or impurity potentials in the nanotube device provides a qualitative explanation of the data.

I. SAMPLE FABRICATION AND MEASUREMENT

The arc-grown MWNTs in these experiments were dispersed from a suspension in dimethyl-formamide on to an oxidized Si wafer on which Au alignment marks had been previously fabricated by electron-beam lithography. High-resolution transmission electron micrographs (TEMs) of the MWNTs show that they consist of about 20–50 concentric tubes covered with a layer of amorphous carbon [Fig. 1(b)]. The MWNTs were typically 2–5 μm long and had diameters in the range of 25–50 nm. The nanotubes were located with respect to the alignment marks using a high-resolution field-emission SEM in the low-voltage mode. Electrodes were patterned by electron-beam lithography to connect selected carbon nanotubes to wirebonding pads. Metallic electrodes (5 nm Ti/50 nm Au) were then evaporated on to the substrate to connect the carbon nanotube to the wirebonding pads. Either four or eight leads were patterned on to the MWNT in order to enable four-terminal measurements of the MWNT. Figure 1(a) shows a scanning electron micrograph (SEM) of a MWNT device with eight contacts. The inset to Fig. 1(a) shows an atomic force microscope (AFM) image of the region of the same device containing the nanotube.

Prior to deposition of the metal, a short oxygen plasma etch (1 or 10 seconds depending on the power used) was performed in order to ensure good electrical contact between the MWNT and the metallic electrode. Without this etch, the electrode-MWNT contact resistance was typically in the range of a few tens of kilohms to a few megohms at room temperature, while with this etch, the contact resistance dropped reproducibly to the range of a few hundred ohms to a few kilohms. Our initial guess as to why the oxygen plasma etch is so efficacious in reducing the contact resistance was that the oxygen plasma etched away the amorphous carbon layer covering the MWNTs. However, TEM images taken after the oxgyen plasma etch showed no reduction in the amorphous carbon layer. Figure 1(b) shows a TEM image of a MWNT after a 10-second oxygen plasma etch. Individual nanotube shells can clearly be seen, along

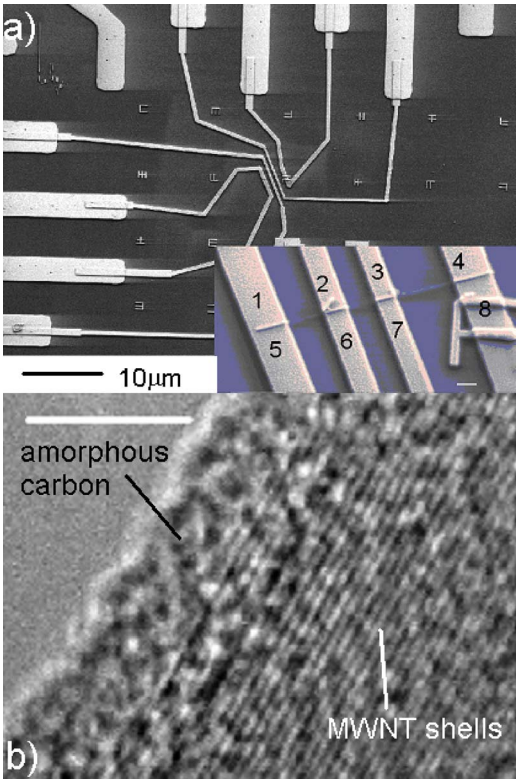

FIG. 1. (Color online) (a) SEM of a typical device, a single MWNT with four contacts. Each contact connects to two electrodes, giving eight electrodes for the device. This enables four-terminal measurements of the contact resistance of the two inner contacts. Inset: SEM image of the central region of the same device, showing the MWNT. The numbers label the current and voltage contacts in different probe configurations as discussed in the text. The size bar is 200 nm. (b) TEM of a MWNT after a typical oxygen plasma etch. The multiple shells of the MWNT as well as the coating of amorphous carbon that survives the etching process can be seen. The size bar is 5 nm.

with the amorphous carbon coating the entire MWNT. However, it should be noted that the amorphous carbon coating could also be due to contamination from the TEM during imaging. Another process by which the oxygen plasma etch might improve the contact resistance is by the introduction of defects on the nanotube surface, as has been suggested by other groups.[18] At this point, we are not sure why the oxygen plasma reduces the contact resistance of the devices. It may be that the oxygen plasma cleaning removes any residual resist left on the carbon nanotube after the development process, while the presence of metastability in the low-contact resistance devices suggests that the reason may well have to do with the introduction of defects near the nanotube-metal contact.

The samples were measured in a ^{3}He refrigerator and a dilution refrigerator. The ^{3}He refrigerator could be inserted into a dewar with a two-axis magnet enabling magnetotransport measurements with the field direction aligned along the tube axis as well as perpendicular to the tube axis. The dilution refrigerator was equipped with a 12-T axial solenoid applying a magnetic field oriented perpendicular to the axis of the MWNTs. The four contacts to each MWNT allowed us to make four-terminal resistance measurements using a homemade ac resistance bridge operating in the frequency range of 11–103 Hz. On samples with eight electrodes, like the sample of Fig. 1, we could also make four-terminal measurements of the contact resistance of the two inner contacts. For differential resistance measurements as a function of dc current bias, a homemade current source with an output impedance greater than 10^{12} Ω was used to apply a dc current in parallel to the ac current applied by the bridge. In performing the experiments, it turned out that the symmetry of the differential resistance with respect to current bias was important. Hence, great care was taken to null out any offset of the current source. With our electronics, the offset could be nulled to the level of 0.2 nA. Using two bridges operating at different frequencies, we could also make simultaneous differential resistance measurements on different parts of the device: for example, the four-terminal resistance of the MWNT and the four-terminal resistance of one contact could be measured simultaneously as a function of dc current bias.

Special care was taken to minimize noise interference from external sources, particularly in the experiments in the dilution refrigerator. No cold filters were used, but π filters with a cutoff frequency of 5 MHz were used to shield every line entering the refrigerator. The signals from the refrigerator were first amplified by battery-operated homemade amplifiers with gains on the order of 100–500. The amplifiers, along with the resistance bridges and current sources were placed in a μ-metal shielded box close to the top of the refrigerator in order to minimize interference from line-frequency sources. Tests were performed to determine the optimum ac current for the measurements: typical ac excitations used were in the range of 0.2–1 nA in order to avoid self-heating. The success of these measures can be seen in the fact that most of the samples measured show strong temperature dependences and no saturation even at the base temperature (15 mK) of the dilution refrigerator.

For the differential resistance measurements on the MWNT devices, the dc current was sent through the same two electrodes as the small ac excitation current, and the resulting ac voltage was measured across the two other metallic electrodes. For example, referring to the electrodes labeled by numbers in the inset to Fig. 1(a), the dc and the ac current could be sent through electrodes 1 and 4, and the resulting ac voltage measured across electrodes 2 and 3. Using the now standard notation for four-terminal measurements, this gave the differential resistance $R_{14,23}=dV_{23}/dI_{14}$ as a function of the dc current I. Similarly, the four-terminal resistances of the two inner electrode-MWNT contacts in the inset to Fig. 1(a) are denoted by dV_{61}/dI_{23} and dV_{47}/dI_{23}. For devices with only four electrodes, the contact resistance was estimated from the measured differences between the two-terminal and four-terminal measurements of the sample and the known resistance of the metallic electrodes. In order to facilitate comparison with theoretical models, we shall plot the conductance $G=1/R$ as a function of the dc bias voltage V_{dc} across the device. This is obtained by numerically integrating the dV/dI vs I curves.

In experiments on our first devices, a gate voltage of order 1 V was applied to the substrate to look for variations in the conductance. However, the conductance had no measurable

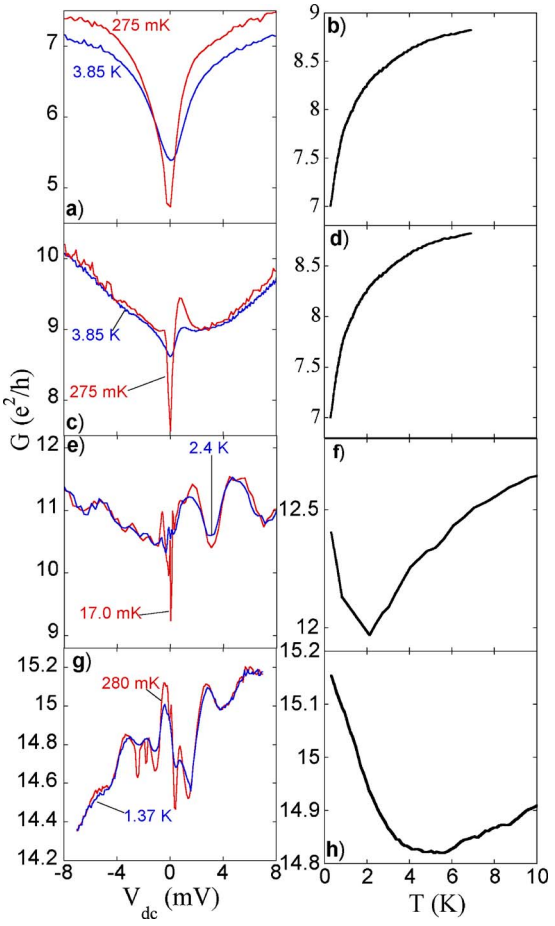

FIG. 2. (Color online) Differential conductance $G=1/(dV/dI)$ vs voltage V_{dc} at two temperatures (left column) and zero-bias conductance vs temperature T for four different MWNT devices in decreasing order of room temperature contact resistance. Each row represents one sample. From top to bottom: (a),(b) sample A: contact resistance 1 kΩ; (c),(d) sample B: contact resistance 900 Ω; (e),(f) sample C: contact resistance 300 Ω; (g),(h) sample D: contact resistance 100 Ω.

dependence on this back gate voltage. This is consistent with the observations of other groups that metallic MWNTs with low-resistance contacts showed no appreciable gate voltage dependence.[5,6] Consequently, in all subsequent experimental runs, the substrate was kept floating.

II. EXPERIMENTAL RESULTS

Figure 2 shows representative behavior of 4 devices out of the more than 14 devices measured. The first column of graphs shows the conductance G as a function of dc voltage bias V_{dc} at two different temperatures; the second column shows the measured zero-bias temperature dependence. The graphs are arranged from top to bottom in order of decreasing contact resistance, from approximately 1 kΩ per contact for the top row to less than a hundred ohms per contact for the bottom row. A clear evolution in G as a function of V_{dc} can be observed. The device with the largest contact resistance shows a conductance that increases monotonically with

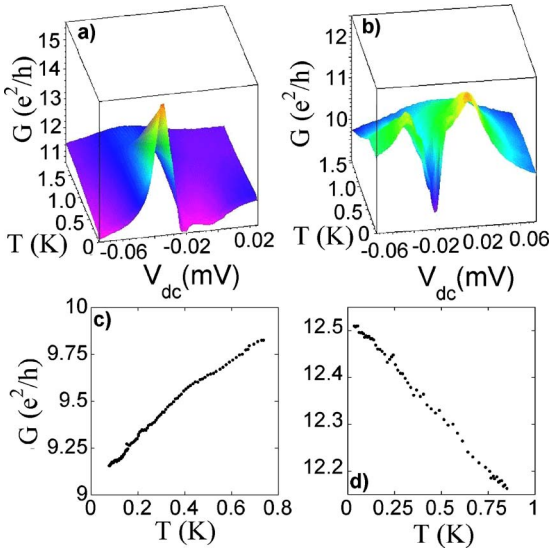

FIG. 3. (Color online) (a),(b) Three-dimensional representation of the differential conductance of sample C as a function of voltage and temperature. Panel (a) is on the first cooldown, at 20 mK, and (b) is on the second cooldown, at 16 mK, after warming the dilution refrigerator to room temperature. (c) and (d) are the corresponding zero-bias temperature dependences.

increasing $|V_{dc}|$, with G at zero bias decreasing with decreasing temperature. This is similar to the zero-bias anomalies observed by other groups, where this behavior has been attributed to Coulomb blockade effects or electron-electron effects in the tunneling regime. (The behavior of devices with contact resistances larger than 1 kΩ is similar.) As we move to devices with lower contact resistances, however, $G(V_{dc})$ begins to show sharp peaks and valleys that have no particular symmetry with respect to $V_{dc}=0$; these features become sharper as the temperature is lowered and appear to be more numerous for devices with lower contact resistances. We note that these features really become prominent only at dilution refrigerator temperatures, which may explain why they have not been observed before in devices measured only down to liquid helium temperatures. With regard to the temperature dependence, devices with higher contact resistances almost invariably show a zero-bias conductance that decreases with decreasing temperature, as can be seen in Figs. 2(b) and 2(d). At first sight, the devices with lower contact resistances appear to show a nonmonotonic temperature dependence, with the conductance decreasing with decreasing temperature at higher temperatures and increasing with decreasing temperature at lower temperatures [Figs. 2(f) and 2(h)]. As we shall see later, however, for devices with low contact resistances, whether the conductance decreases or increases with decreasing temperature depends on whether a maximum or minimum in the conductance occurs at zero bias: if a maximum occurs, the conductance will increase with decreasing temperature; if a minimum occurs, the conductance will decrease with decreasing temperature.

In fact, the same device could show both types of behavior on different cooldowns. Figure 3(a) shows the conductance of sample C of Fig. 2 as a function of temperature over a limited range of V_{dc} on a three-axis plot. The major feature

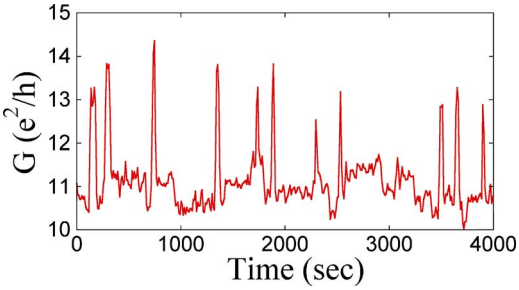

FIG. 4. (Color online) Time dependence of the zero-bias conductance of sample C, taken at 35 mK.

in the data is the presence of a large conductance peak at around $V_{dc}=-25$ μV that grows in amplitude with decreasing temperature. Near zero bias, however, there is a local minimum in conductance; since this minimum also grows in amplitude with decreasing temperature, the zero-bias conductance of the device decreases with decreasing temperature, as shown in Fig. 3(c). Figures 3(b) and 3(d) show similar data on the same device taken after the refrigerator had been warmed to room temperature and cooled back down again. As can be seen, the conductance characteristics have changed drastically. Where there was a maximum in the conductance, there is now a minimum. Near zero bias, there is now a maximum in conductance; consequently, the conductance increases with decreasing temperature, as shown in Fig. 3(d). Indeed, we found that for some devices, it was not necessary to warm to room temperature to see a change in the transport characteristics. In these devices, the conductance would frequently change on a time scale of a few hours to a few days, which made obtaining consistent data over a long period of time difficult. Figure 4, which shows the zero-bias conductance of sample C as a function of time, shows an example of this metastable behavior. The conductance switches between two states on a time scale of minutes. While most of our devices did not switch as frequently as this, the majority of them showed changes in the conductance on thermal cycling.

The fluctuations in the conductance as a function of V_{dc} and the time dependence of the conductance are strongly reminiscent of conductance fluctuations in diffusive metallic and semiconducting devices, where they are associated with quantum interference of quasiparticles that are scattered by impurities, defects, or surfaces.[19,20] In the diffusive case, changing V_{dc} is equivalent to changing the energy E of the quasiparticles, which in turn changes the phase of the interference. The time dependence of the conductance can arise from the movement of even a single impurity over a distance greater than $1/k_F$, where k_F is the Fermi wave vector of the electrons.[21–23] A shift of an impurity over this length scale shifts the phases of quasiparticles scattering off that particular impurity by $\sim\pi$, which leads to a change in conductance of order e^2/h in a fully coherent device. If the impurity is metastable, i.e., if it moves between two positions as a function of time, the conductance will also show a corresponding time dependence.

The phase of the interfering quasiparticles can also be modified by applying a magnetic field. Figure 5(a) shows the

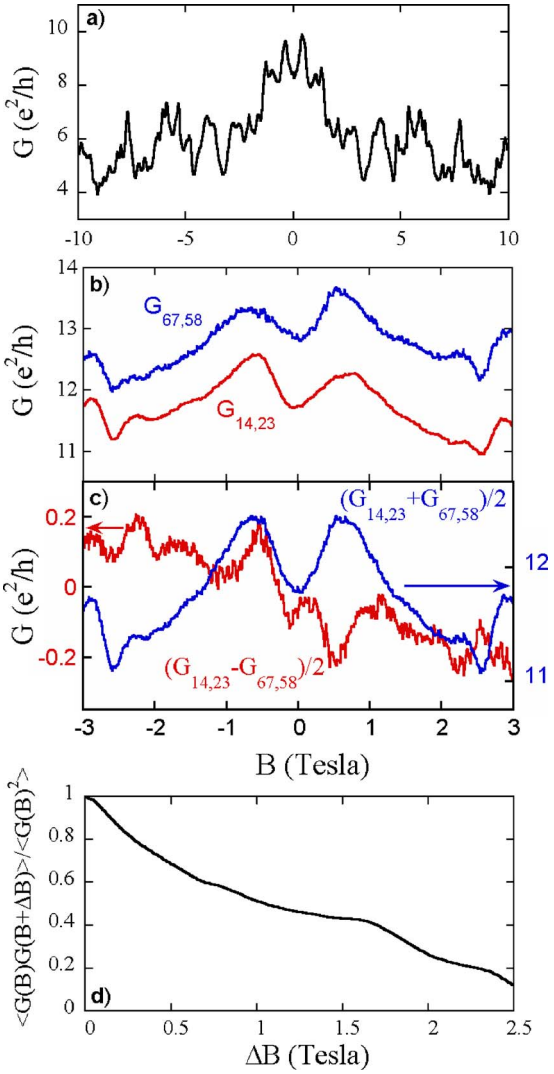

FIG. 5. (Color online) (a) Magnetoconductance of sample C at 25 mK. (b) Low-field magnetoconductance of the same device at low fields with two different measurement configurations as noted. $G_{67,58}$ has been shifted up by 1 e^2/h for clarity. (c) The average of the sum and difference of the two traces shown in (b), demonstrating the symmetric and antisymmetric combinations obtained using the Landauer-Büttiker relations. (d) Autocorrelation function of the magnetoconductance data of (a). The correlation field B_c is 1.05 T.

magnetoconductance of sample C as a function of the magnetic field. Large variations in the conductance as a function of the magnetic field can be observed. On this field scale, the conductance looks symmetric with respect to the magnetic field B. A closer examination of the region near $B=0$, however, reveals that the magnetoconductance is asymmetric with respect to the magnetic field, as expected for a four-terminal measurement of a mesoscopic device, and indeed obeys the the Landauer-Büttiker symmetry relations.[16,17] Figure 5(b) shows the low-field magnetoconductances $G_{14,23}$ and $G_{67,58}$ measured simultaneously as a function of the magnetic field B. Both traces are clearly asymmetric. Taking the combinations $(G_{14,23}+G_{67,58})/2$ and $(G_{14,23}-G_{67,58})/2$, as shown in Fig. 5(c), gives curves that are essentially symmetric and antisymmetric with respect to B, as predicted by

the Landauer-Büttiker relations.[24] It should be noted that the fact that the amplitude of the conductance fluctuations in the antisymmetric part of the magnetoconductance is large is an indication that quasiparticle phase coherence extends from the nanotube into the electrodes. Theoretically, this is because the antisymmetric contribution arises from the two-coordinate Diffuson or Cooperon propagator, where one coordinate of the propagator is in the part of the device common to both the current and voltage paths, and one coordinate is in a current or voltage lead.[25]

From this brief qualitative look at the data from our MWNT devices, it would seem as if the results can be explained by the physics of quantum transport in a diffusive system. However, a more probing qualitative examination and a detailed quantitative analysis show several inconsistencies. First, in looking at the $G(V_{dc})$ curves [Figs. 2(c), 2(e), and 2(g)], it can be seen that the amplitude of the conductance fluctuations increases only in certain narrow ranges in dc bias with decreasing temperature, rather than over the whole range of V_{dc}. For example, in Fig. 2(c), there is almost no change in the conductance outside the range -2 mV $< V_{dc} < 2$ mV in going from 3.85 K to 0.275 K, while the conductance within this voltage range shows large changes. Similar behavior can be seen in the data of Figs. 2(e) and 2(g). Now the amplitude of conductance fluctuations in diffusive systems is expected to grow with decreasing temperature. However, the amplitude should grow over the *entire* voltage range, which it clearly does not. (The energy scale for fluctuations is determined by the Thouless energy.) Second, it should be noted that the rms amplitude of the conductance fluctuations is larger than e^2/h: for example, the rms amplitude of the conductance fluctuations in Fig. 5(a) as calculated from the autocorrelation function is 1.3 e^2/h. In itself, a conductance fluctuation amplitude larger or comparable to e^2/h is not unusual in diffusive samples, where the phase coherence length L_ϕ is longer than the length L of the device; in which case, the amplitude of the conductance fluctuations scales as $(e^2/h)(L_\phi/L)^2$.[26] However, assuming that the fluctuations seen in Fig. 5(a) are due to quantum interference in a diffusive sample, one can estimate L_ϕ from the correlation field B_c of the magnetoconductance, $L_\phi \sim (h/e)/(B_c W)$, where W is the width of the wire.[20] B_c is determined by taking the autocorrelation function of the conductance $\langle G(B)G(B+\Delta B)\rangle$, being defined as the magnetic field difference ΔB at which the autocorrelation falls to half its $\Delta B=0$ value. From the autocorrelation function of the magnetoconductance data of Fig. 5(a), shown in Fig. 5(d), $B_c \sim 1.05$ T, giving $L_\phi \sim 80$ nm with the estimated width W of the MWNT being 50 nm. This is about a quarter of the typical distance of 300 nm between the voltage probes of our MWNT devices. Consequently, the maximum amplitude of the conductance fluctuations should be $e^2/h(L_\phi/L)^{3/2} \sim 0.14e^2/h$ or smaller, rather than $\sim 1.3e^2/h$. (We note in passing that the value of $\sim 0.14e^2/h$ is closer to the amplitude of conductance fluctuations observed in diffusive MWNTs by other groups.[11,12]) While this analysis shows that quantum interference in a *diffusive* system is an unlikely explanation for our results, we believe that quantum interference in a quasiballistic system in the presence of a few impurities is quite likely, as we shall show shortly.

III. QUANTUM INTERFERENCE IN A QUASIBALLISTIC SYSTEM: FANO RESONANCES

In searching for a model to explain the voltage-dependent differential conductance of the MWNT devices, it is useful to enunciate the specific characteristics of the data that any model will need to describe. The most evident is the presence of sharp minima and maxima in the conductance at specific values of voltage across the device, which leads us to consider a resonance-type phenomenon. The model will have to explain the presence of both minima and maxima in conductance. Some devices show only one such minimum or maximum [e.g., Fig. 2(c)], while other devices show many minima and maxima [e.g., Fig. 2(g)]. The minima and maxima occur at all values of voltage, not just at $V_{dc}=0$, as can be seen from Fig. 3. Finally, the peaks or dips are quite often asymmetric with respect to the maximum or minimum of conductance. These distinguishing characteristics rule out some more conventional models such as the Kondo effect to explain our data.[27]

The model that we believe best explains the data from our MWNT devices is based on the interference between a quasiparticle path that is directly transmitted an appreciable distance along the MWNT and a path that is transmitted via a resonant state with a well-defined energy E_0, the so-called Fano resonance.[28] In what follows, we shall the notation of Clerk *et al.* in their discussion of the Fano resonance as applied to mesoscopic systems.[29] The transmission amplitude of the direct channel is written as $t_d=\sqrt{T_d}e^{i\alpha}$, while the energy-dependent transmission amplitude of the resonant channel is given by $t_r(E)=z_r\Gamma/[2(E-E_0)+i\Gamma]$. Here E is the energy of the incoming quasiparticle. Without the factor z_r, this results in the usual expression for transmission T_r through a resonant state of energy E_0 and intrinsic width Γ, $\sim \Gamma^2/[4(E-E_0)^2+\Gamma^2]$. Similarly, the transmission of the direct channel by itself is given simply by $|t_d|^2=T_d$, independent of E. The interference between these two transmission paths is taken into account by taking the sum of t_r and t_d to determine the total transmission coefficient, $T_t=|t_d+t_r|^2$. α determines the relative phase between the direct path and the resonant path, while the ratio of T_d to z_r determines the relative amplitude of the two terms. The energy-dependent conductance can be cast in the conventional Fano form[28]

$$G_{Fano}(E) = \frac{2e^2}{h}T_t = \frac{2e^2}{h}T_d\frac{|2(E-E_0)+q\Gamma|^2}{4(E-E_0)^2+\Gamma^2}, \qquad (1)$$

where $q=i+z_r e^{-i\alpha}/\sqrt{T_d}$ is the complex Fano factor.

The conductance described by the equation above has all the right characteristics to explain the structure we see in the differential conductance of our devices. Since the energy of the resonant state E_0 is not necessarily 0, the resonance can occur at finite values of the voltage V_{dc}. In the limit $E \gg \Gamma$, there is no contribution to the transmission from the resonant state, so the conductance reduces to $G=(2e^2/h)T_d$, the conductance of the direct channel alone, as one would expect off

resonance. On resonance ($E=E_0$), the conductance depends on the phase difference α between the direct and resonant paths. For $\alpha=0$ or $\alpha=\pi$, $T_t=T_d+z_r^2$, which corresponds to the incoherent transmission of the direct and resonant paths in parallel. For $\alpha=-\pi/2$, one obtains $T_t=(\sqrt{T_d}+z_r)^2$, while for $\alpha=\pi/2$, one obtains $T_t=(\sqrt{T_d}-z_r)^2$. Thus, depending on α, one can get a minimum or a maximum in conductance near resonance. In general, the resonance line shape described by Eq. (1) is asymmetric with respect to the minimum or maximum of the conductance. If T_d and z_r are of order unity, one would expect changes in the conductance of order of a few e^2/h, but only at voltages in the vicinity of the resonance, as seen in the experiment. Multiple resonant states would lead to multiple maxima or minima, as seen for example in the data of Fig. 2(g). Finally, if the resonant state is caused by an impurity that results in a local perturbation in the potential seen by quasiparticles in the MWNT device, movement of the impurity would result in a change in the phase difference α between the direct and resonant paths, leading to a change in conductance of order of a few e^2/h as a function of time, as seen in the time-dependent data of Fig. 4.

Fano resonances in MWNT devices have been reported by two other groups.[30,31] Kim *et al.*[30] measured the conductance of devices incorporating crossed MWNTs and observed a Fano resonance in two of their devices. Since a Fano resonance was never found in devices without a MWNT cross, they associated the Fano resonance with the presence of a MWNT cross, although the mechanism that gave rise to a resonant state was not elucidated. Yi *et al.*[31] measured the conductance of crosses consisting of metal electrodes patterned across MWNT bundles. In two of these devices, they observed a nonmonotonic behavior of the conductance near zero bias, which they ascribed to a resonance arising from interference between a Kondo resonance and nonresonant channels. However, the nature of the Kondo resonance and why it did not occur at the Fermi energy as observed in the experiments was not made clear. More recently, Fano resonances have been observed in single-walled nanotubes[32] (SWNTs). In these experiments, it was speculated that the interference might occur between two transport channels in a single SWNT, or between transport channels on different nanotubes in a SWNT bundle. In all these experiments, the metastable behavior we observe was not reported.

In analyzing the differential conductance of our own devices quantitatively, we shall concentrate on sample C whose data is shown in Fig. 3(a) and 3(b), since we have the most comprehensive temperature dependence for this device. Since only one peak or dip is prominent, these data are also easier to analyze than the data of other devices, for example, the device of Fig. 2(g), where multiple resonances must be fit. Even so, we still have the problem of subtracting the background differential conductance, the part of the differential conductance not associated with the resonance. This background is relatively temperature independent [see, for example, Figs. 2(c), 2(e), and 2(g)]. Nevertheless, there are small changes in the background conductance with temperature that do occur, so that one cannot simply subtract the differential conductance at higher temperatures to obtain the temperature dependence of the resonance at lower temperatures. Consequently, we have instead used a numerical technique to subtract the background at each temperature. This technique involves cutting out from the differential conductance the data in the voltage range over which the resonance occurs, taking the Fourier transform of the remaining curve, filtering the Fourier transform to remove the high-frequency components, and then reverse Fourier transforming to obtain the background. The result of this process is shown as the dashed lines for the conductance peak and dip represented by the solid lines in Fig. 6. The numerical process employed clearly involves some assumptions about how the background behaves, but we believe that the resulting slowly varying background is a more realistic approximation than simply assuming a flat background over the same voltage range.

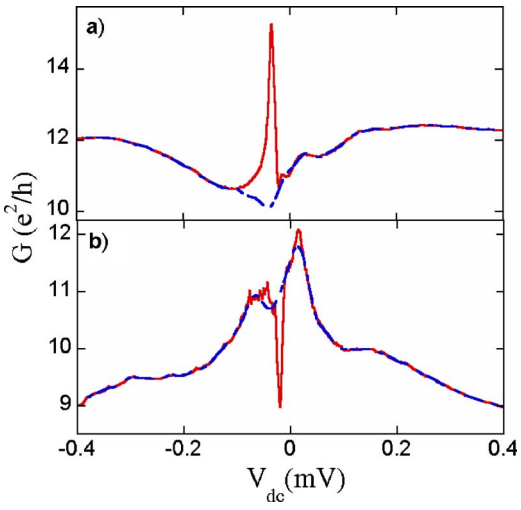

FIG. 6. (Color online) (a) Differential conductance data for sample C on the first cooldown, taken at 20 mK. The dashed line shows the background calculated from the Fourier transform, as described in the text. (b) Similar curves for the conductance dip observed on the second cooldown of sample C at 16 mK.

Perforce, the value of the conductance far off resonance after the background subtraction process described above would be 0, since we have also subtracted any off-resonance contribution of the direct channel of the Fano resonance, the contribution corresponding to $G_d=(2e^2/h)T_d$. What is the value of T_d? The background conductance of this sample is roughly 10 e^2/h. In the Landauer picture, we could ascribe this conductance to five channels that are transmitted ballistically, which of course is highly unlikely. More likely is a larger number of channels that each have transmission coefficients T less than unity. In truth, we do not really care how many channels contribute to the background conductance; we are more concerned with how many channels interfere coherently with the resonant channel. However, we believe that the total number of conducting channels is small; otherwise, the fluctuations resulting from the interference of the coherent channels would be swamped by the contribution of the incoherent channels and, hence, would be much smaller than we observe. This picture is consistent with the conclusion by other groups that only the outer shells in a MWNT contacted by external electrodes contribute to the conductance.[5]

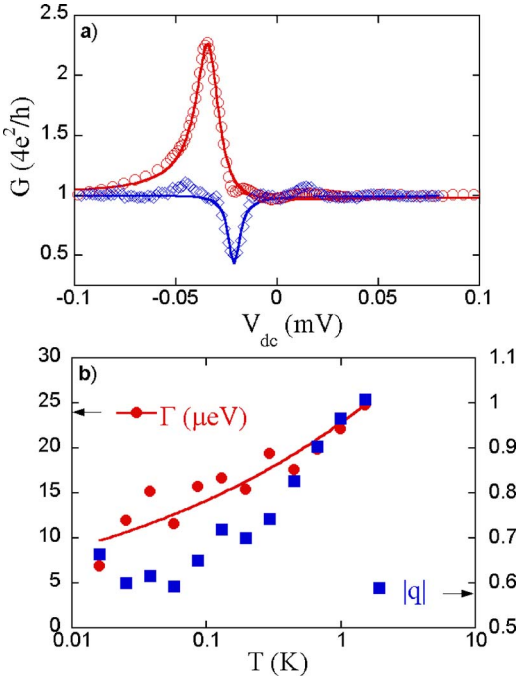

FIG. 7. (Color online) (a) Open symbols; data for the conductance peak and dip of Fig. 6 after the subtraction of the backgrounds shown by the dashed curves in Fig. 6, with an offset of $4e^2/h$ added. Solid lines, fits to the Fano formula, Eq. (1). Fitting parameters for the dip are $|q|=0.66$, $\theta=1.61$, and $\Gamma=6.9$ μeV, and are for the conductance peak $|q|=1.50$, $\theta=1.69$, and $\Gamma=13.6$ μeV. (b) Temperature dependence of the fitting parameters Γ and $|q|$ for the conductance dip of (a). The solid line is a fit to the data, giving $\Gamma=22.9\times T^{0.21}$ μeV.

Since only one resonance peak or dip is prominent in the voltage range shown in Fig. 6, it is a safe assumption that only one resonant state contributes. Now suppose only one direct channel with transmission $T_d=1$ interferes coherently with the resonant state. We would then have to add an offset of $2e^2/h$ to the background-subtracted curves. With this offset, however, the conductance of the dip at its minimum would fall below zero, which is unphysical. Of course, the conductance at the minimum is slightly sensitive to the subtraction process; however, we have explored a range of parameters such as the voltage range over which the resonance is assumed to occur and the frequency cutoff in the Fourier filter, but we still have the same problem. If we assume that two channels interfere coherently with the resonant state, each with a conductance of $2e^2/h$, the conductance curve should be offset by $(4e^2/h)$. In this case, the conductance at the minimum of the dip no longer goes below 0. One could also assume three or more channels interfering coherently with the resonant state. We think this is less likely, however, so in what follows, we will assume only two direct channels interfering with the resonant state. This assumption also agrees with the concept of only two channels being present in a single metallic nanotube shell.

The open symbols in Fig. 7(a) show the resulting background-subtracted data with an offset of $4e^2/h$ for both the conductance peak and the conductance dip of Figs. 3(a) and 3(b) at 20 mK and 16 mK, respectively, along with the best fits to the Fano functional form, Eq. (1). For the dip, the magnitude of the complex Fano factor from the fit, $|q|=0.65$, while the phase θ of q is nearly $\pi/2$ (1.61). This value for θ corresponds to a phase difference of about $\alpha=\pi/2$ (1.507) between the direct and resonant channels. Remembering that T_d is 2 by the choice of our offset, the value of $|q|$ then should be $1-z_r/\sqrt{T_d}=0.3$, assuming the amplitude of the resonant channel $z_r=1$. For the peak, $|q|=1.50$, θ is 1.69 (again close to $\pi/2$). In this case, α is closer to $-\pi/2(-1.2)$, giving an expected amplitude of $|q|-1+z_r/\sqrt{T_d}=1.7$. More exact calculations give numbers that are closer to the fitted values obtained.

Figure 7(b) shows the fitted values of $|q|$, the linewidth Γ and the phase θ as a function of temperature for the conductance dip of Fig. 7(a). θ is essentially constant at $\pi/2(1.58\pm0.06)$ over the entire temperature range. Both $|q|$ and Γ increase with increasing temperature. Now the Fano formula [Eq. (1)] is for zero temperature: at finite temperature, one would expect a thermal broadening of the form

$$G(V,T)=\int G_{Fano}(E)\left(-\frac{\partial f(E-eV)}{\partial E}\right)dE, \qquad (2)$$

where $f(E)$ is the Fermi function. At temperatures $T\gg\Gamma/k_B$, the effective linewidth of the resonance should be approximately $3.5\,k_B/T$. At $T=1$ K, for example, the effective linewidth should be ~300 μeV instead of the much smaller value of ~22 μeV that we obtain. For this reason, our attempts to fit to the temperature-dependent equation, Eq. (2), were unsuccessful. It should be noted that Kim *et al.*[30] also found an effective linewidth Γ that was approximately a factor of 5 smaller than expected. However, their linewidth scaled linearly with temperature, while ours shows a much weaker temperature dependence of the form $\sim T^{1/5}$. Kim *et al.* suggested that the narrower linewidth observed in their experiments might be due to the four-terminal nature of the measurements. Although no further explanation was given in their paper, we believe their idea is that the inner voltage leads measure only a fraction of the total voltage applied across the device by the current leads. However, we do not think that this is the correct explanation for the narrower linewidths observed in our experiments. If the transport of the quasiparticles from one current lead to its corresponding voltage lead is ballistic, then the voltage measured at the voltage lead should be the same as the voltage applied at the current lead. If it is not, then the voltage lead measures the relevant voltage applied across the device. A straightforward test of this hypothesis is to apply the current using the two inner leads and measure the voltage with the two outer leads. In this configuration, there is nominally no voltage drop between a current lead and its corresponding voltage lead along the nanotube since the voltage lead draws no current. Our measurements of devices using this configuration have shown peaks with linewidths narrower than $3.5\,k_BT$, so this cannot be the origin of the narrow linewidths we observe. This issue requires further study.

What is the origin of the resonant state that contributes to the Fano resonance? The metastable nature of the conductance seen in some of our devices suggests that it might be

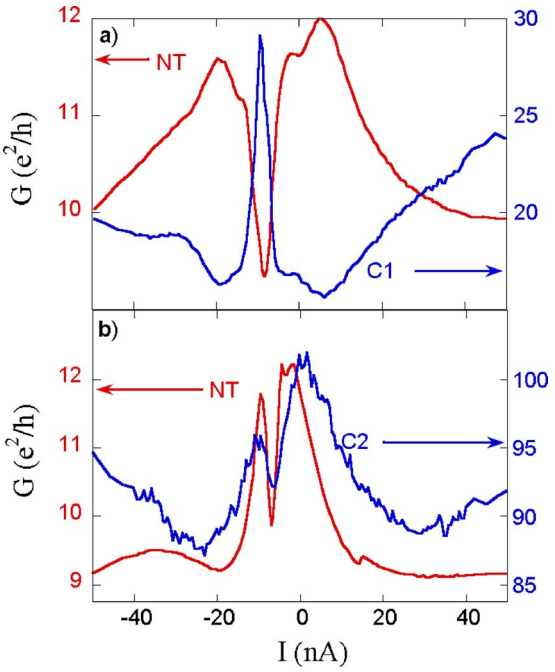

FIG. 8. (Color online) Simultaneous measurements of the four-terminal conductance of the contacts of sample C and the MWNT device itself at 25 mK. (a) MWNT conductance and the left contact conductance (see Fig. 1). (b) MWNT conductance and the right contact conductance.

due to impurities that perturb the potential seen by the quasiparticles, leading to bound states in some part of the sample. Where are these impurities located? Due to the inherently nonlocal nature of phase-coherent transport, it is hard to localize the position of the impurities. Bias-dependent four-terminal measurements of the contact resistance taken simultaneously with the four-terminal resistance of the MWNT device also show sharp peaks and dips in the conductance at exactly the same values of bias as the peaks and dips seen in the MWNT resistance. Figure 8(a) shows the conductance of the left inner contact and the MWNT conductance taken simultaneously; Fig. 8(b) shows the conductance of the right inner contact and the MWNT taken simultaneously. In the former figure, there is an anticorrelation of the conductance of the contact and the MWNT (the correlation is −0.96), while in the latter figure, there is a correlation of the conductance with the conductance of the MWNT (correlation 0.81). Now, one might argue that the anticorrelation seen in Fig. 8(a) clearly shows that the impurity is located at the metal-MWNT interface of this contact; however, this picture does not agree with the observation that the conductance of the second contact also shows a strong correlation with the conductance of the MWNT. A more likely explanation is that all three conductances are sensitive to the resonant state since the phase coherence extends throughout this region of the MWNT and into the probes (as the asymmetries seen in the magnetoconductance indicate). Thus, it is hard to tell exactly where the impurity or impurities are located. A similar situation occurs in the case of time-dependent conductance fluctuations, where it is not possible to determine the position of a fluctuating impurity within a phase-coherent region.[23]

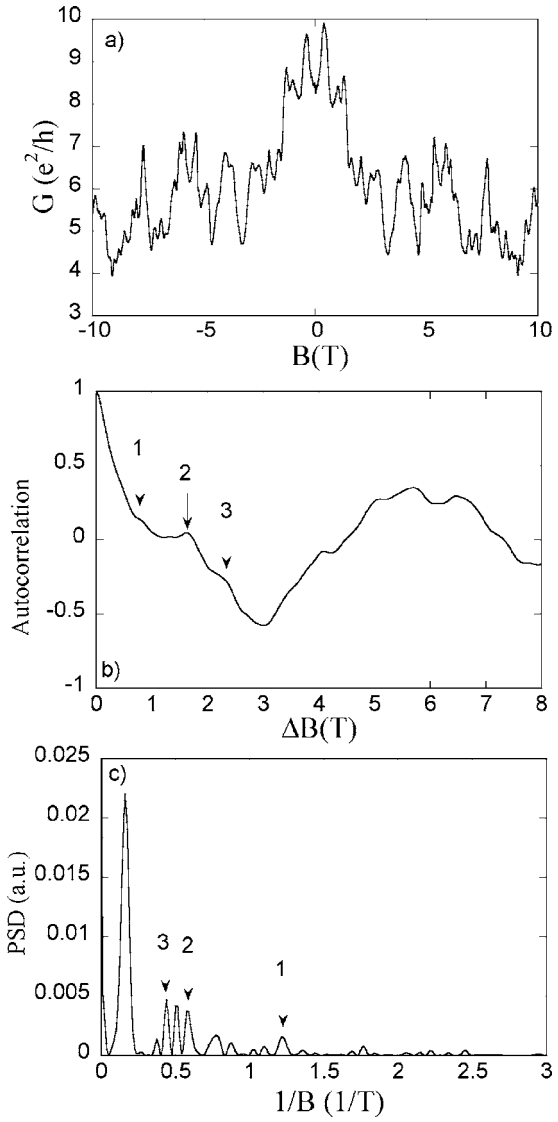

FIG. 9. (a) Magnetoconductance of sample C, at 25 mK. (b) Autocorrelation function of the data in (a), $\langle G(B)G(B+\Delta B)\rangle/\langle G(B)^2\rangle$, after a sixth-order polynomial background has been subtracted. (c) The PSD of the magnetoconductance data of (a), after a sixth-order polynomial background has been subtracted. The arrows in (b) mark the period of magnetoconductance oscillations; the corresponding arrows in (c) mark the frequency.

As we noted earlier, quantum interference effects can be modulated by a magnetic field. For Fano resonances, this has been elegantly demonstrated using semiconducting quantum dots embedded in Aharonov-Bohm interferometers, where the Fano resonance could be modulated periodically by an externally applied magnetic field.[33] Although the interference paths in our devices are not as clearly defined, we believe that the large oscillations in the magnetoconductance observed in our devices is due to an Aharonov-Bohm modulation of the interference between the directly transmitted and resonant channels contributing to the Fano resonance. First, as we discussed earlier, the amplitude of the variations in the conductance observed as a function of the magnetic field are much larger than those expected from conductance fluctuations in a diffusive conductor, given the phase-coherence

length estimated from the magnetoconductance data. Second, superimposed on top of the background fluctuations of the magnetoconductance are periodic oscillations. This can be seen clearly by looking at the autocorrelation functions and the Fourier transforms of the magnetoconductance. Figure 9 shows the magnetoconductance, autocorrelation function and power spectral density (PSD) of the magnetoconductance of sample C whose data have been shown already in Fig. 5, at 25 mK. In order to accentuate the periodic components, a sixth-order polynomial background has been subtracted from the data before performing the autocorrelation and Fourier transforms. The largest peak in the PSD corresponds to the large background oscillation with period of around 5.5 T. We believe that this large-scale oscillation may be associated with modifications in the density of states, as has been reported by other groups.[13] Clear peaks are also seen in the autocorrelation function corresponding to oscillations with smaller periods; the first three have been marked by arrows in the plots and the peaks in the PSD corresponding to these periods have been similarly tagged. (Note that other periods are also seen.) At first sight, these oscillations appear to correspond to different periods. Closer inspection reveals that the period of peaks 2 and 3 are multiples of the period of peak 1, which has a period of 0.8 T. Similar behavior is seen in other samples. We believe that this period corresponds to a modulation of the phase of the Fano resonance by the magnetic field. The period of 0.8 T corresponds to the penetration of a single normal flux quantum h/e over length scale of approximately 100 nm, given an estimated width of 50 nm of the carbon nanotube. This is perhaps the extent of the potential perturbation caused by the impurity.

In summary, MWNT devices with low-resistance contacts measured at millikelvin temperatures show a wealth of structure in their differential conductance as a function of the bias applied across the device. This structure arises from Fano resonances in the MWNT. The metastable nature of the differential conductance suggests that the resonant states that give rise to the Fano resonances are created by impurities that can move as a function of thermal cycling and as a function of time.

ACKNOWLEDGMENTS

We thank the group of R. P. H. Chang for providing the nanotubes used in these experiments and D. A. Dikin and R. Piner for the TEM and AFM images of the nanotubes. Funding for this work was provided by a NASA/MSFC Phase II SBIR, Contract No. NAS8-02102, and by the NSF through Grant No. NSF-NER 0403590.

*Corresponding author. Electronic address: v-chandrasekhar@northwestern.edu

[1] S. Frank, P. Poncharal, Z. L. Wang, and W. A. de Heer, Science **280**, 1744 (1998).

[2] A. Urbina, I. Echeverría, A. Pérez-Garrido, A. Díaz-Sánchez, and J. Abellán, Phys. Rev. Lett. **90**, 106603 (2003).

[3] L. Langer, V. Bayot, E. Grivei, J. P. Issi, J. P. Heremans, C. H. Olk, L. Stockman, C. Van Haesendonck, and Y. Bruynseraede, Phys. Rev. Lett. **76**, 479 (1996).

[4] M. Baxendale, V. Z. Mordkovich, S. Yoshimura, and R. P. H. Chang, Phys. Rev. B **56**, 2161 (1997).

[5] A. Bachtold, C. Strunk, J. P. Salvetat, J. M. Bonard, L. Forró, T. Nussbaumer, and C. Schönenberger, Nature (London) **397**, 673 (1999).

[6] C. Schönenberger, A. Bachtold, C. Strunk, J. P. Salvetat, and L. Forró, Appl. Phys. A **69**, 283 (1999).

[7] A. Fujiwara, K. Tomiyama, H. Suematsu, M. Yumura, and K. Uchida, Phys. Rev. B **60**, 13492 (1999).

[8] K. Liu, P. Avouris, R. Martel, and W. K. Hsu, Phys. Rev. B **63**, 161404(R) (2001).

[9] N. Kang, J. S. Hu, W. J. Kong, L. Lu, D. L. Zhang, Z. W. Pan, and S. S. Xie, Phys. Rev. B **66**, 241403(R) (2002).

[10] R. Tarkiainen, M. Ahlskog, A. Zyuzin, P. Hakonen, and M. Paalanen, Phys. Rev. B **69**, 033402 (2004).

[11] B. Stojetz, C. Hagen, C. Hendlmeier, E. Ljubovic, L. Forró, and C. Strunk, New J. Phys. **6**, 27 (2004).

[12] B. Stojetz, C. Miko, L. Forró, and C. Strunk, Phys. Rev. Lett. **94**, 186802 (2005).

[13] Jeong-O Lee, J. R. Kim, J. J. Kim, J. Kim, N. Kim, J. W. Park, K. H. Yoo, and K. H. Park, Phys. Rev. B **61**, R16362 (2000).

[14] C. Schönenberger and A. Bachtold, Phys. Rev. B **64**, 157401 (2001).

[15] Z. Zhang, D. A. Dikin, R. S. Ruoff, and V. Chandrasekhar, Europhys. Lett. **68**, 713 (2004).

[16] A. D. Benoit, S. Washburn, C. P. Umbach, R. B. Laibowitz, and R. A. Webb, Phys. Rev. Lett. **57**, 1765 (1986).

[17] M. Büttiker, Phys. Rev. Lett. **57**, 1761 (1986).

[18] See, for example, A. Bachtold, M. Henny, C. Tarrier, C. Strunk, C. Schonenberger, J. P. Salvetat, J. M. Bonard, and L. Forró, Appl. Phys. Lett. **73**, 274 (1998); R. Tarkiainen, M. Ahlskog, A. Zyuzin, P. Hakonen, and M. Paalanen, *ibid.* **69**, 33402 (2004).

[19] P. A. Lee and A. D. Stone, Phys. Rev. Lett. **55**, 1622 (1985); P. A. Lee, A. D. Stone, and H. Fukuyama, Phys. Rev. B **35**, 1039 (1987); B. L. Al' tshuler, Pis'ma Zh. Eksp. Teor. Fiz. **41**, 530 (1985) [JETP Lett. **41**, 648 (1985)].

[20] S. Washburn and R. A. Webb, Adv. Phys. **35**, 375 (1986), and references cited therein.

[21] S. Feng, P. A. Lee, and A. D. Stone, Phys. Rev. Lett. **56**, 1960 (1986).

[22] B. L. Al' tshuler and B. Z. Spivak, Pis'ma Zh. Eksp. Teor. Fiz., **42**, 363 (1985) [JETP Lett. **42**, 447 (1985)].

[23] B. Golding, N. M. Zimmerman, and S. N. Coppersmith, Phys. Rev. Lett. **68**, 998 (1992); N. O. Birge, B. Golding, and W. H. Haemmerle, Phys. Rev. B **42**, 2735 (1990).

[24] One should really take the combinations $G_{14,23}$ and $G_{23,14}$ in order to determine the symmetric and antisymmetric combinations. However, this would involve taking the curves sequentially since the same contacts must be used, and this was difficult given the metastability of the device. The combination $G_{67,58}$ uses the same metallic electrodes as $G_{23,14}$ [see the inset to Fig. 1(a)].

[25] V. Chandrasekhar, P. Santhanam, and D. E. Prober, Phys. Rev. B **44**, 11203 (1991).
[26] A. Benoit, C. P. Umbach, R. B. Laibowitz, and R. A. Webb, Phys. Rev. Lett. **58**, 2343 (1987).
[27] J. Nygard, D. H. Cobden, and P. E. Lindelof, Nature **408**, 342 (2000).
[28] U. Fano, Phys. Rev. **124**, 1866 (1961).
[29] For a good discussion of Fano resonance as applied to mesoscopic systems, see A. A. Clerk, X. Waintal, and P. W. Brouwer, Phys. Rev. Lett. **86**, 4636 (2001).
[30] J. Kim, J. R. Kim, Jeong-O Lee, J. W. Park, H. M. So, N. Kim, K. Kang, K. H. Yoo, and J. J. Kim, Phys. Rev. Lett. **90**, 166403 (2003).
[31] W. Yi, L. Lu, H. Hu, Z. W. Pan, and S. S. Xie, Phys. Rev. Lett. **91**, 076801 (2003).
[32] B. Babic and C. Schönenberger, Phys. Rev. B **70**, 195408 (2004).
[33] K. Kobayashi, H. Aikawa, S. Katsumoto, and Y. Iye, Phys. Rev. Lett. **88**, 256806 (2002).